

Production of ultracold Cs*Yb molecules by photoassociation

Alexander Guttridge,^{1,*} Stephen A. Hopkins,¹ Matthew D. Frye,²
John J. McFerran,³ Jeremy M. Hutson,^{2,†} and Simon L. Cornish^{1,‡}

¹*Joint Quantum Centre (JQC) Durham-Newcastle, Department of Physics,
Durham University, South Road, Durham, DH1 3LE, United Kingdom.*

²*Joint Quantum Centre (JQC) Durham-Newcastle, Department of Chemistry,
Durham University, South Road, Durham, DH1 3LE, United Kingdom.*

³*Department of Physics, University of Western Australia, 6009 Crawley, Australia*
(Dated: March 9, 2024)

We report the production of ultracold heteronuclear Cs*Yb molecules through one-photon photoassociation applied to an ultracold atomic mixture of Cs and Yb confined in an optical dipole trap. We use trap-loss spectroscopy to detect molecular states below the Cs($^2P_{1/2}$) + Yb(1S_0) asymptote. For $^{133}\text{Cs}^{174}\text{Yb}$, we observe 13 rovibrational states with binding energies up to ~ 500 GHz. For each rovibrational state we observe two resonances associated with the Cs hyperfine structure and show that the hyperfine splitting in the diatomic molecule decreases for more deeply bound states. In addition, we produce ultracold fermionic $^{133}\text{Cs}^{173}\text{Yb}$ and bosonic $^{133}\text{Cs}^{172}\text{Yb}$ and $^{133}\text{Cs}^{170}\text{Yb}$ molecules. From mass scaling, we determine the number of bound states supported by the $2(1/2)$ excited-state potential to be 154 or 155.

I. INTRODUCTION

Ultracold polar molecules are a promising platform for the study of new forms of quantum matter [1–3], cold controlled chemistry [4, 5] and tests of fundamental physics [6–10]. The electric dipole moment possessed by polar molecules can be exploited to engineer controllable long-range dipole-dipole interactions, which have many applications in quantum simulation [11–13], quantum computation [14] and the study of quantum many-body physics [15, 16]. Many of these applications require gases of ground-state molecules with high phase-space density confined in optical traps or lattices. Whilst direct laser cooling of molecules has undergone spectacular recent progress [17–20], the molecules produced in these experiments are currently limited to low phase-space densities. However, high-phase-space-density gases of ultracold molecules can be produced from ultracold mixed-species gases of alkali-metal atoms using magnetoassociation on a Feshbach resonance followed by optical transfer to deeply-bound states.

High-phase-space-density gases of KRb [21], RbCs [22, 23], NaK [24] and NaRb [25] molecules have been produced in the $^1\Sigma$ ground-state using this approach and the first steps towards realising the richness of ultracold molecular systems have been demonstrated using such bi-alkali molecules [26–28]. At the same time, the quest for new species of ultracold molecules possessing a magnetic dipole moment, in addition to an electric dipole moment, has become a field of burgeoning interest, with both $^2\Sigma$ [29–34] and $^3\Sigma$ molecules [35] being pursued. The additional degree of freedom possessed

by these molecules allows quantum simulation of a wide range of two-dimensional lattice spin models [36] and tuning of collisions and chemical reactions [37].

Following the success of the association technique in bi-alkali experiments, the association of an alkali-metal atom and a closed-shell atom is a promising approach for the production of $^2\Sigma$ molecules. Magnetoassociation of such molecules is complicated in comparison to the bi-alkali case due to the singlet ground state of the closed-shell atom which precludes the existence of broad Feshbach resonances. However, the weak distance dependence of the hyperfine coupling, caused by the proximity of the second atom, is predicted to produce usable Feshbach resonances [38, 39] in these systems, with CsYb one of the most promising candidates [40]. Such resonances have recently been observed experimentally in the RbSr system [41], but magnetoassociation remains unexplored.

Light-assisted techniques such as photoassociation (PA) [42] and stimulated Raman adiabatic passage (STIRAP) [43] offer alternative approaches for the production of ground-state molecules in these systems which are not reliant on the existence of suitable Feshbach resonances. Photoassociation is a technique where a colliding atom pair is excited to a rovibrational level of an excited molecular potential, forming an excited molecule. The subsequent decay of the excited molecule is determined by the Franck-Condon factor (FCF), which dictates the branching ratios for molecular decay into energetically lower states, including the continuum. By choosing an excited vibrational level with a favourable Franck-Condon overlap with the ground state, photoassociation can be used as a method of producing ground-state ultracold molecules [44–48]. Alternatively, the coherent transfer of a colliding atom pair to a bound vibrational level of the molecular ground state is also possible, as has been investigated in Sr_2 [49, 50]. The two techniques can be combined using photoassociation to populate a high-lying vibrational level followed by coher-

* alexander.guttridge@durham.ac.uk

† j.m.hutson@durham.ac.uk

‡ s.l.cornish@durham.ac.uk

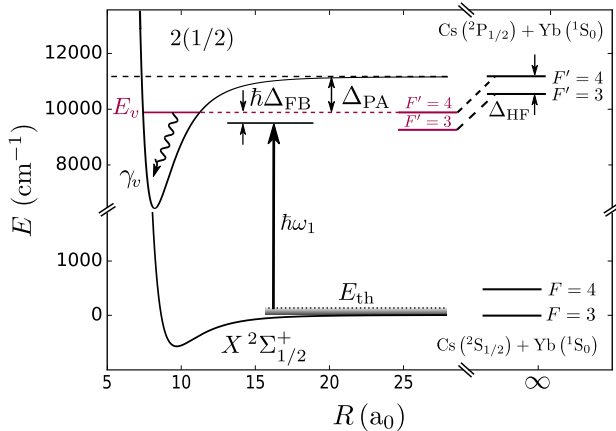


FIG. 1. One-photon photoassociation. When $\hbar\omega_1 = E_v$ ($\hbar\Delta_{\text{FB}} = 0$) a pair of colliding ground-state Cs and Yb atoms are associated to form a CsYb molecule in a rovibrational level of the electronically excited $2(1/2)$ molecular potential. The binding energy of this rovibrational level, Δ_{PA} , is measured with respect to the Cs D_1 line which the $2(1/2)$ potential approaches asymptotically. The molecular curves plotted here are adapted from Ref. [52]. The hyperfine splitting shown on the right is not to scale.

ent transfer to the absolute ground state [51]. The first step towards identifying viable routes for the creation of molecules using these all-optical approaches involves sensitive photoassociation measurements of near-threshold bound states to determine the long-range potential of the excited molecular state. This technique is illustrated in Fig. 1 for CsYb and is explored in this work.

In this paper we report the production of ultracold heteronuclear Cs*Yb molecules using one-photon PA applied (initially) to an ultracold atomic mixture of ^{133}Cs and ^{174}Yb confined in an optical dipole trap (ODT). We present measurements of the binding energies of rovibrational states up to 500 GHz below the $\text{Cs}(^2P_{1/2}) + \text{Yb}(^1S_0)$ asymptote. The electronic state at this threshold is designated $2(1/2)$ to indicate that it is the second (first excited) state with total electronic angular momentum $\Omega = 1/2$ about the internuclear axis. It correlates at short range with the $1^2\Pi_{1/2}$ electronic state in Hund's case (a) notation [52], but at long range the $^2\Pi_{1/2}$ and $^2\Sigma_{1/2}$ states are strongly mixed by spin-orbit coupling.

We fit an extended version of the LeRoy-Bernstein near-dissociation expansion formula to the measurements and characterize the long-range potential in the $2(1/2)$ excited state. We investigate the role of hyperfine coupling in Cs*Yb molecules by studying the hyperfine splitting of the observed lines and show a dependence on the internuclear separation. Finally, we expand the scope of our investigation by measuring the PA spectra of an additional 3 CsYb isotopologs, $^{133}\text{Cs}^{173}\text{Yb}$, $^{133}\text{Cs}^{172}\text{Yb}$ and $^{133}\text{Cs}^{170}\text{Yb}$. Using mass scaling, we determine the number of bound states supported by the $2(1/2)$ molecu-

lar potential. These results represent a critical first step towards the coherent production of molecules in the electronic ground-state by a two-photon process.

II. EXPERIMENTAL SETUP

Photoassociation measurements are typically performed in either a magneto-optical trap (MOT) or an optical dipole trap (ODT). We use an ODT as our experiment employs a single Zeeman slower that prevents continuous loading of Cs and Yb into a dual-species MOT [53, 54]. The use of an ODT has the advantage that the internal states of the atoms are better defined, the temperature is lower and the interspecies density is higher than in typical MOT experiments. However, measurements in the ODT are performed using destructive absorption imaging to determine the number of atoms remaining after exposure to the PA light. PA spectra must therefore be built up by repeating the experiment multiple times whilst stepping the frequency of the PA light. This makes broad frequency scans much more time-consuming in comparison to MOT measurements where the MOT fluorescence can be continuously monitored as the PA laser frequency is scanned.

The ODT used in this work is formed from the output of a broadband fibre laser (IPG YLR-100-LP) with a wavelength of 1070(3) nm, and consists of two beams crossed at an angle of 40° with waists of 33(4) μm and 72(4) μm . The measured Yb (Cs) trap frequencies are 240 (750) Hz radially and 40 (120) Hz axially. The trap depths for the two species are $U_{\text{Yb}} = 5 \mu\text{K}$ and $U_{\text{Cs}} = 85 \mu\text{K}$. We typically load the ODT with a mixture of 8×10^5 ^{174}Yb atoms at $T_{\text{Yb}} = 1 \mu\text{K}$ in the 1S_0 ground state and 7×10^4 Cs atoms at $T_{\text{Cs}} = 6 \mu\text{K}$ in the absolute ground state $^2S_{1/2} |F=3, m_F=+3\rangle$. A detailed description of the experimental apparatus and the routine for the preparation of this mixture is given in Refs. [53–56].

The PA light is derived from a Ti:Sapphire laser (M Squared SolisTiS), the main output of which is passed through an acousto-optic modulator for fast intensity control and coupled into a fibre which carries the light to the experimental table. The PA light is focused onto the trapped atomic mixture with a waist of 150 μm and is polarized parallel to the applied magnetic field in order to drive $\Delta m_F = 0$ transitions. The hyperfine structure of the weakly bound molecular states is similar to that of the atomic state (see Fig. 1). The strengths of transitions to these molecular states are dictated by the dipole matrix elements as in the atomic case [57]. The choice of polarization allows the excitation to molecular levels in both hyperfine manifolds.

The frequency of the PA light is both stabilized and calibrated using a high-finesse optical cavity, the length of which is stabilised to a Cs atomic transition using the Pound-Drever Hall method [58]. PA light sent to the cavity passes through a broadband fibre electro-

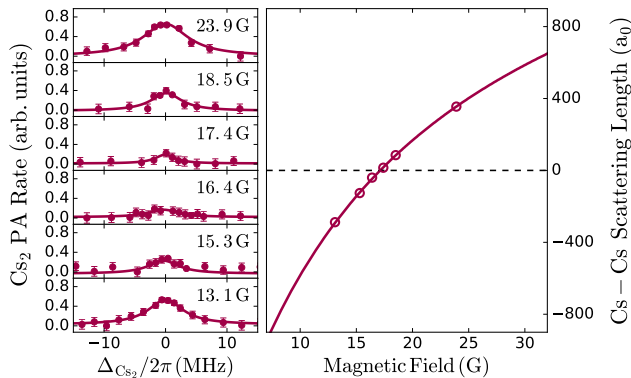


FIG. 2. Modification of Cs_2 photoassociation rate using a Feshbach resonance. The left panel shows Cs_2 photoassociation rates as a function of detuning from the $0_u^+ v = 136$ line for varying magnetic field strengths. The right panel shows the Cs scattering length as a function of magnetic field [61] (for clarity, narrow Feshbach resonances at 14.4 G, 15.1 G and 19.9 G are not shown). The red circles show the scattering lengths at magnetic fields corresponding to the measurements on the left.

optic modulator (EOM) (EOSPACE PM-0S5-10-PFA-PFA-895) modulating the light with frequency sidebands. We utilize the ‘electronic sideband’ technique [59, 60] to allow continuous tunability of the PA laser frequency; by stabilising one of the sidebands to a cavity transmission peak, the frequency of the carrier may be tuned over the 748.852(5) MHz free spectral range (FSR) of the cavity by changing the modulation frequency applied to the EOM. Precise frequency calibration with respect to the Cs D_1 transition is then achieved by counting cavity fringes from the D_1 transition and including the rf modulation offsets of the carrier. In practise a commercial wavemeter (Bristol 671A) is used to identify the specific cavity fringe used to stabilise the PA laser frequency.

Due to the large difference in polarizability at the wavelength of our ODT and the collision properties of Cs and Yb, we can currently prepare only a mixture with a large number imbalance in favor of Yb [56]. Therefore, Cs^*Yb PA resonances are detected by loss of Cs atoms from the ODT. Unfortunately, the Cs atoms are also affected by off-resonant scattering of the PA light, leading to non-resonant loss and optical pumping into the upper hyperfine manifold ($F = 4$). To improve the signal-to-noise ratio, we use a pulse of imaging light on the Cs $6S_{1/2}, F = 4 \rightarrow 6P_{3/2}, F' = 5$ transition to remove any atoms off-resonantly pumped into the upper hyperfine level prior to detection of the population in $|F = 3, m_F = +3\rangle$.

A larger issue is the existence of the many Cs_2 PA resonances below the D_1 transition [62–66], making identification of CsYb lines challenging. However, due to the tunability of the scattering length of Cs we can tune the magnetic field to suppress the Cs_2 PA rate, as shown in Fig. 2. This effect is well understood in the context

of Feshbach-Optimized Photoassociation (FOPA) [67–69] and is due to the modification of the scattering wavefunction in the vicinity of a Feshbach resonance which, in turn, modifies the Franck-Condon overlap with a specific excited vibrational level. The effect is typically used to enhance the PA rate of a transition. Here, however, we use the effect to suppress the Cs_2 PA rate by operating at a magnetic field of 16.4(2) G when searching for CsYb PA lines. This is not expected to modify the CsYb PA rate as the predicted Feshbach resonances in this system are very sparse and narrow [40]. Note that this magnetic field properly suppresses Cs_2 resonances over most of the range of detunings explored here, but, due to the oscillatory nature of the ground-state wavefunction, for larger detunings it can enhance the PA rate [67].

We typically measure the CsYb PA lines by illuminating the trapped atomic mixture with a pulse of PA light for 300 ms at an intensity of $I = 0.1 - 10 \text{ W/cm}^2$ (depending on the strength of the transition). The ODT light is then turned off and the number of atoms is measured using resonant absorption imaging. Short scans (comparable to the cavity FSR) are performed by tuning the modulation frequency of the fibre EOM, measuring the Cs number with each frequency step. We stitch together longer scans by locking the PA laser frequency to sequential modes of the cavity.

III. EXPERIMENTAL RESULTS

A. $^{133}\text{Cs}^{174}\text{Yb}$ Photoassociation

A typical CsYb PA spectrum is shown in Fig. 3 as a function of the detuning Δ_{FB} from the free-bound transition. The figure displays the $n' = -11$ line, where we label the lines by numbering the vibrational levels of the $2(1/2)$ state below its threshold, starting from $n' = -1$. Explicitly, $n' = v - v_{\text{max}} - 1$, where v is the vibrational quantum number and v_{max} is the vibrational quantum number of the least-bound state. As the levels we observe are all close to threshold, n' is relatively easy to determine, but we cannot label the states by v as v_{max} is initially unknown.

When the frequency of the PA laser is tuned into resonance with a CsYb line we observe a loss of Cs atoms due to the formation of Cs^*Yb molecules. We verify that the detected features are CsYb resonances (and not Cs_2 resonances) by repeating the scan in the absence of Yb. To keep the density and temperature of the Cs atoms comparable to the measurement taken with Yb, we simply remove Yb from the ODT with a pulse of light resonant with the $^1S_0 \rightarrow ^1P_1$ transition immediately before the sample is illuminated by the PA light. The disappearance of the feature in the absence of Yb (red trace in Fig. 3) confirms the existence of a CsYb PA resonance.

For all vibrational levels we observe a second PA feature which is red-detuned by approximately the hyperfine splitting of the Cs $6P_{1/2}$ level. For the weakly bound vi-

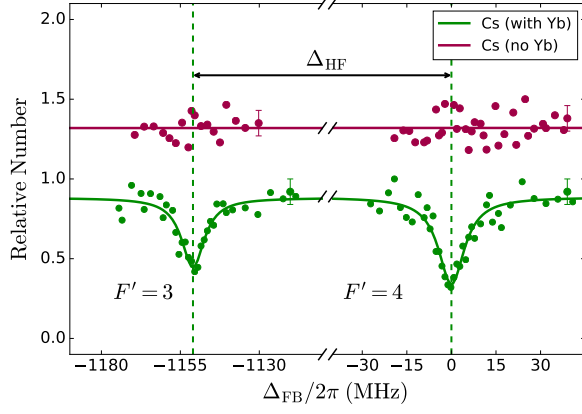


FIG. 3. Observation of the photoassociation resonance for $n' = -11$ of $^{133}\text{Cs}^{*174}\text{Yb}$. Relative number of Cs atoms remaining after a 300 ms pulse of PA light versus detuning from the $F' = 4$ line (Δ_{FB}). The green (red) trace shows the photoassociation spectra of Cs with (without) the presence of Yb in the dipole trap. The red (Cs only) trace has been offset for clarity. The statistical error in the atom number is shown by the error bars on the right hand side. The dashed green line shows the centres of the CsYb PA resonance for each hyperfine component.

brational states investigated here, the Cs*Yb molecules inherit the properties of the two free atoms; as such we identify the two lines by the quantum numbers $F' = 4$ and $F' = 3$ corresponding to the hyperfine structure in the excited state of Cs. The rovibrational levels are best described by the classic form of Hund's case (e) introduced by Mulliken [70], in which the total atomic angular momentum F' here) couples to the rotational angular momentum R' to form a resultant F' . This uncommon coupling case was first observed for HeKr⁺ [71] and has also been found in RbYb [72, 73]. In our case, all rovibrational levels observed have $R' = 0$ because of the low temperature of the initial atomic mixture.

Table I lists the binding energies of all observed vibrational levels relative to the Cs $6S_{1/2}, F = 3 \rightarrow 6P_{1/2}, F' = 4$ atomic transition. These measurements were performed at a magnetic field of 2.2(2) G to reduce uncertainty caused by the Zeeman shift of the molecular state when measuring the hyperfine splitting. The binding energies are obtained using the difference in EOM modulation frequencies and number of cavity FSRs between the PA transition and the atomic transition, as outlined earlier. The uncertainty due to the stabilisation of the cavity length is the dominant source of uncertainty for the majority of the measured binding energies. The exception is the $n' = -19$ line, where the observed FWHM linewidth of 130(10) MHz leads to a larger uncertainty in determining the line centre. All the other features have linewidths approximately equal to the linewidth of the Cs D_1 transition, as shown in Fig. 3.

The strength of the transition is determined by observ-

n'	$\Delta_{\text{PA}}/2\pi$ (GHz)	Normalized strength	$\Delta_{\text{HF}}/2\pi$ (MHz)
Cs	0	N/A	1168(2)
-7	-17.244(3)	1.0(2)	1162(1)
-8	-26.473(3)	0.4(3)	1157(3)
-9	-38.567(3)	0.40(5)	1154(1)
-10	-53.932(3)	0.17(1)	1151(1)
-11	-72.973(3)	0.19(1)	1147(1)
-12	-96.091(3)	0.091(8)	1142(2)
-13	-123.678(3)	0.10(2)	1139(1)
-14	-156.117(3)	0.045(4)	1131(1)
-15	-193.772(3)	0.06(2)	1127(1)
-16	-236.991(3)	0.013(2)	1120(1)
-17	-286.098(4)	0.05(1)	1115(2)
-18	not observed		
-19	-402.867(8)	0.0063(4)	1071(8)
-20	-472.384(6)	0.0033(6)	1084(6)

TABLE I. Measured binding energies of vibrational levels in the $2(1/2)$ electronically excited state of $^{133}\text{Cs}^{*174}\text{Yb}$. Binding energies are given for the $F' = 4$ level and are measured relative to the Cs D_1 atomic transition [$6S_{1/2}, F = 3 \rightarrow 6P_{1/2}, F' = 4$]. The uncertainties quoted are 1σ uncertainties [74]. The observed strengths of the lines are normalized to that of the strongest PA line, $n' = -7$. The hyperfine splittings are the measured separations of the $F' = 4$ and $F' = 3$ components. The measured atomic value is in agreement with the literature value of the hyperfine splitting of the $m_F = +3$ levels in a 2.2 G magnetic field, 1169.272(81) [75].

ing the loss of Cs atoms as a function of intensity of PA light. We observe an exponential decay of the Cs atom number as a function of intensity. The decay constant extracted from the exponential fit is normalized to that of the $n' = -7$ level and given in Table I.

Figure 4 shows the measured binding energies of all one-photon PA transitions found for $^{133}\text{Cs}^{*174}\text{Yb}$. Vibrational levels are observed with binding energies of order 20 to 500 GHz detuned from the Cs D_1 line. These measured binding energies are relatively small compared to the depth of the potential (≈ 200 THz), so the positions of the vibrational levels are determined by the long-range potential. The potential curve for a pair of atoms can be described at sufficiently large internuclear distance R by an inverse-power series

$$V(R) = D - \frac{C_n}{R^n} - \frac{C_m}{R^m} - \dots, \quad (1)$$

where $V(R)$ is the potential as a function of internuclear distance, D is the threshold energy, and C_n and C_m are long-range coefficients. At long range, the CsYb $2(1/2)$ potential is dominated by the van der Waals $n = 6$ term. The long-range coefficients may be extracted from PA spectra using near-dissociation expansion formulas. The

simplest and most widely used of these expansions is the Le Roy-Bernstein (LRB) formula [76] which links the energy E_v of the vibrational state v to the asymptotic form ($D - C_n/R^n$) of the potential

$$E_v \simeq D - \left(\frac{v_D - v}{B_n} \right)^{2n/(n-2)}, \quad (2)$$

where v_D is the non-integer vibrational quantum number at dissociation and B_n is a constant that depends on the reduced mass and the leading long-range power n . In practice, it is more convenient to express $v_D - v$ in terms of n' and v_{frac} , the fractional part of v_D ; for a single isotope, v_{max} does not affect the predicted level positions.

In searching for PA lines, we modelled our data using the LRB equation (for $n = 6$) and used the fitted parameters to predict more deeply bound levels. This technique yielded accurate predictions for levels up to $n' = -17$, with the measured binding energies typically lying within a few hundred MHz of the predicted values. For the more deeply bound levels $n' = -19$ and $n' = -20$, the measured line frequencies were far from the extrapolated values and the $n' = -18$ level was not observed at all. The non-observation of the $n' = -18$ level may be due to a small Franck-Condon factor or that the level is located outside the range searched (± 2 GHz from the prediction) or coincided with a Cs_2 transition. We did not search further due to the ~ 30 s load-detection cycle associated with conducting the measurements.

The middle panel of Fig. 4 shows the residuals from the fit of our PA measurements to the LRB equation. The $n' = -19$ and $n' = -20$ levels are outliers and so not included in any of our fits. It is clear from the residuals that the standard LRB equation does not fully describe our measured PA spectra. The structure of the residuals suggests that a model including higher-order terms would give a better fit to the results. Indeed, the more strongly bound levels with binding energies around 300 GHz are deep enough to be sensitive to the non-asymptotic, short-range character of the potential for our measurement precision.

To model the PA spectra better, we also fit them using an extended version of the LRB equation, specifically Eq. (39) in Ref [77]. The extended version allows the inclusion of one higher-order dispersion coefficient (we use $m = 8$) and a mass-dependent parameter γ which accounts for the non-asymptotic, short-range part of the potential. The bottom panel of Fig. 4 shows the residuals of the fit to the extended LRB equation. The inclusion of the extra terms significantly improves the fit to the results. The reduced chi-squared of the extended fit is $\chi^2_\nu = 2.3$, much better fit than the standard LRB equation which gives $\chi^2_\nu = 275$. The best-fit parameters for the extended fit are $C_6 = 10.1(1) \times 10^3 E_h a_0^6$, $C_8 = 5.0(2) \times 10^6 E_h a_0^8$, $v_{\text{frac}} = 0.696(6)$ and $\gamma^{-1} = h \times 3.4(1) \times 10^2$ GHz.

When fitting to either model, the residuals for $n' = -19$ and -20 are over 30 times larger than that of the

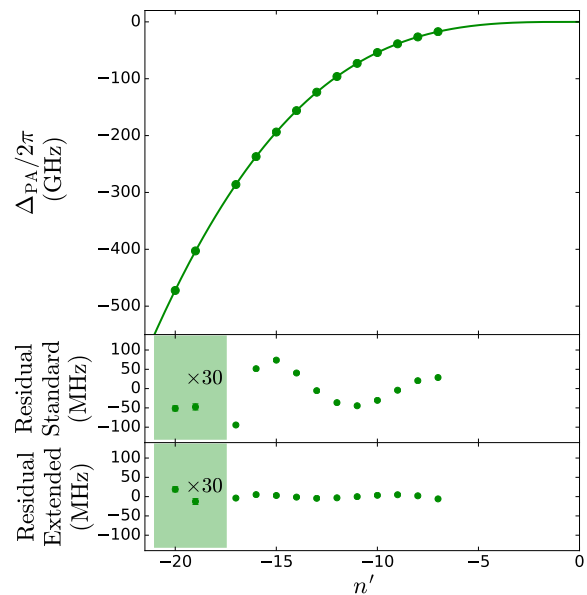


FIG. 4. Binding energies of vibrational levels of $^{133}\text{Cs}^{174}\text{Yb}$ on the $2(1/2)$ excited-state potential by one-photon photoassociation spectroscopy. Upper: The detuning of observed $F' = 4$ PA resonances are plotted against the vibrational quantum number counted from dissociation, n' . The dissociation energy corresponds to the $|6S_{1/2}, F = 3 \rightarrow 6P_{1/2}, F' = 4\rangle$ atomic transition. The solid green line shows a fit to the data using the extended Le Roy-Bernstein equation (see text). The lower two panels compare the residuals for the fits using the standard and extended Le Roy-Bernstein equations. There is clear discrepancy for $n' = -19$ and $n' = -20$ whose residuals are 30 times larger than those plotted on the figure. Most of the error bars are much smaller than the data points.

other levels. These levels may be perturbed by mixing with vibrational levels in a different electronic state [78]. The shift could also be caused by the broadband dipole trapping light coupling to a higher electronic state. The $n' = -19$ line is extremely broad in comparison to other observed lines; it has a FWHM of 130(10) MHz, over eight times the linewidth of $n' = -16$ (FWHM = 15(2) MHz) at the same light intensity. We have not been able to observe any levels beyond $n' = -20$, although we have searched a moderate ± 1 GHz range around the predicted positions. As can be seen from the residuals for the deepest observed states in Fig. 4, the disagreement with the LRB fit results in an increasingly large search space, which is very time consuming to explore.

As discussed earlier, the CsYb spectra display hyperfine structure associated with the Cs atom (see Fig. 3). We present the measured hyperfine splitting for all the observed levels in Table I and we illustrate the dependence of the hyperfine coupling on internuclear distance in Fig. 5. We approximate the effective internuclear distance R_{eff} for each transition as the Condon point, where the transition energy is equal to the spacing between

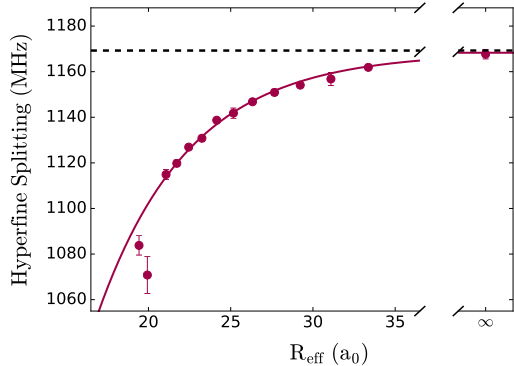


FIG. 5. Measured hyperfine splitting as a function of the effective internuclear distance, R_{eff} (see text for details). The horizontal dashed line shows the Cs atomic hyperfine splitting of the $m_F = +3$ levels in the $6P_{1/2}$ state at a magnetic field of 2.2(2) G [75, 79]. The solid line is an exponential fit to guide the eye.

the two curves. The points show the measured hyperfine splitting of the $F' = 4$ and $F' = 3$ levels of each vibrational level. We find that as the binding energy increases and the internuclear separation reduces, the strength of the Cs hyperfine coupling decreases. This is due to the perturbation of the electronic wave function of the Cs atom by the presence of the closed-shell Yb atom [38]. A similar effect in the ground state has been observed to produce Feshbach resonances in RbSr [41]. The deepest bound level $n' = -20$ exhibits a hyperfine splitting of $\Delta_{\text{HF}} = 1084(6)$ MHz, a reduction of almost 100 MHz from the atomic value. The hyperfine splitting of $n' = -19$ is smaller than this value but this may be due to mixing of vibronic states in other electronic states causing a modification of the coupling.

B. Extension to other CsYb Isotopologs

Ytterbium has numerous stable isotopes, both bosonic and fermionic, that can be trapped and cooled to ultracold temperatures [80–85]. Within the Born-Oppenheimer approximation, the interaction potential is mass-independent but the positions of vibrational levels depend on the reduced mass.

In WKB quantization, the non-integer quantum number at dissociation, $v_D = v_{\text{max}} + v_{\text{frac}}$, is given by $v_D = \Phi/\pi - 1/2$, where Φ is the phase integral

$$\Phi = \int_{R_{\text{in}}}^{\infty} [(2\mu/\hbar^2)(D - V(R))]^{1/2} dR. \quad (3)$$

Here R_{in} is the location of the inner classical turning point, μ is the reduced mass and $V(R)$ is the interaction potential. The dependence on μ allows us to determine

Yb Isotope	n'	$\Delta_{\text{PA}}/2\pi$ (MHz)	Residual (MHz)	
			$N = 154$	$N = 155$
173	-9	-36.117(3)	-10	6
173	-10	-50.877(3)	-10	11
173	-11	-69.246(3)	-15	10
173	-12	-91.633(3)	-19	12
173	-13	-118.427(3)	-23	13
173	-14	-150.014(3)	-29	14
173	-15	-186.762(3)	-38	11
172	-8	-22.740(5)	-14	10
172	-11	-65.614(4)	-21	28
172	-13	-113.258(4)	-45	26
170	-12	-103.338(3)	15	150
170	-14	-166.489(3)	55	241

TABLE II. Measured binding energies of vibrational levels in the $2(1/2)$ molecular potential for different isotopologs of $^{133}\text{CsYb}$. The binding energies quoted are for the $F' = 4$ level and are measured relative to the Cs D_1 atomic transition $|6S_{1/2}, F = 3 \rightarrow 6P_{1/2}, F' = 4\rangle$. The residuals presented are from the extended LRB model with $N = 154$ or $N = 155$.

the number of bound states $N = v_{\text{max}} + 1$ by comparing binding energies for different isotopologs.

The measured binding energies of $^{133}\text{Cs}^{173}\text{Yb}$, $^{133}\text{Cs}^{172}\text{Yb}$ and $^{133}\text{Cs}^{170}\text{Yb}$ are tabulated in Table II. The routines used to obtain PA spectra for these isotopologs are similar to that presented for $^{133}\text{Cs}^{174}\text{Yb}$, with the only significant difference in the preparation of the ultracold Yb sample. Slight changes are required to the MOT, ODT loading and evaporative cooling routines to address the different requirements of each Yb isotope due to variations in abundance, intraspecies scattering length and hyperfine structure (for fermionic ^{173}Yb). The $^{133}\text{Cs}^{173}\text{Yb}$ and $^{133}\text{Cs}^{170}\text{Yb}$ measurements take place in identical trapping conditions to $^{133}\text{Cs}^{174}\text{Yb}$. The initial mixture contains 3×10^5 ^{173}Yb or 4×10^5 ^{170}Yb atoms at $T_{\text{Yb}} = 1 \mu\text{K}$ and 5×10^4 Cs atoms at $T_{\text{Cs}} = 6 \mu\text{K}$. The large negative scattering length of ^{172}Yb ($a_{172-172} = -600 a_0$) [86] complicates the evaporative cooling of Yb; we therefore halt the evaporation around $T_{\text{Yb}} = 4 \mu\text{K}$ to prevent a substantial loss of Yb atoms due to 3-body inelastic collisions. PA for $^{133}\text{Cs}^{172}\text{Yb}$ is performed on a mixture of 5×10^5 ^{172}Yb atoms at $T_{\text{Yb}} = 4 \mu\text{K}$ and 7×10^4 Cs atoms at $T_{\text{Cs}} = 12 \mu\text{K}$. In this new trapping arrangement the Yb (Cs) trap frequencies are 380 (1100) Hz radially and 80 (240) Hz axially. The light shift due to this tighter trapping arrangement has been accounted for in the binding energies presented in Table II and leads to a larger uncertainty on the ^{172}Yb measurements.

To determine N from the measured binding energies of the four isotopologs we use a mass-scaled version of the extended LRB model. The values of C_6 and C_8 are the same for all isotopologs. However, v_D is proportional

to $\sqrt{\mu}$, and so v_{frac} varies between isotopologs. γ is also proportional to $\sqrt{\mu}$ [77], but this variation is much less important than that for v_{frac} . For a chosen value of N , we can use the parameters fitted to Cs^{174}Yb to predict binding energies for the other isotopologs and calculate χ_ν^2 . It is possible to refit the parameters with multiple isotopologs, but this makes little quantitative difference and produces the same qualitative conclusions.

The binding energies for Cs^{172}Yb and Cs^{173}Yb are well predicted by the parameters obtained for Cs^{174}Yb with $N = 155$, giving $\chi_\nu^2 = 12$. This compares with $\chi_\nu^2 = 40$ and 158 for $N = 154$ and 156 respectively. However, including Cs^{170}Yb gives $\chi_\nu^2 = 36$ for $N = 154$ and 322 for $N = 155$. It thus appears that the results for the different isotopologs are inconsistent with a single-potential model; the deviations are outside the experimental errors and clearly non-statistical.

It is possible that the lines for one or more isotopes are affected by an isotope-dependent perturbation, most likely due to a level of the $3(1/2)$ electronic state that dissociates to the $6^2P_{3/2}$ state of Cs. Such a perturbation is not encapsulated in our model and characterizing it would require extensive further work. Nevertheless, we can conclude that the number of bound states supported by the $2(1/2)$ potential is either 154 or 155. This is within 10% of the 145 bound states predicted for this potential by Menailava and Shundalau [52].

IV. CONCLUSION

We have produced ultracold Cs^*Yb molecules using photoassociation on an atomic mixture trapped in an optical dipole trap. We have measured the binding energies of 13 vibrational levels of the electronically excited $2(1/2)$ state of $^{133}\text{Cs}^{174}\text{Yb}$ and fitted dispersion coefficients for its interaction potential at long-range near the $\text{Cs } 6^2P_{1/2}$ asymptote. The low temperatures and well-defined inter-

nal states of the atoms in the optical dipole trap allow us to measure the hyperfine splitting of the molecules associated with the $\text{Cs } 6^2P_{1/2}$ state. For more deeply bound Cs^*Yb molecules we observe a decrease in the hyperfine splitting compared to the bare Cs atom. In addition, we measure the binding energies of a number of vibrational levels of $^{133}\text{Cs}^{173}\text{Yb}$, $^{133}\text{Cs}^{172}\text{Yb}$ and $^{133}\text{Cs}^{170}\text{Yb}$. By applying mass scaling, we determine the number of bound states supported by the $2(1/2)$ potential of $^{133}\text{Cs}^{174}\text{Yb}$, which correlates at short range with the $1^2\Pi_{1/2}$ potential, to be 154 or 155. $^{133}\text{Cs}^{173}\text{Yb}$ and $^{133}\text{Cs}^{172}\text{Yb}$ also have this number of bound states, but $^{133}\text{Cs}^{170}\text{Yb}$ has one fewer bound states.

The improved understanding of the electronically excited state will be pivotal in the creation of ground-state CsYb molecules. The measurements presented here are the starting point for two-photon photoassociation to near-threshold levels of the $X^2\Sigma_{1/2}^+$ ground-state potential and for all-optical approaches such as STIRAP to produce molecules in the absolute ground state [49, 50]. Two-photon PA will also allow precise determination of the interspecies scattering lengths and the prediction of Feshbach resonances suitable for magnetoassociation. Ground-state CsYb molecules may find future applications in the fields of ultracold chemistry, precision measurement and quantum simulation.

ACKNOWLEDGMENTS

We acknowledge support from the UK Engineering and Physical Sciences Research Council (grant number EP/P01058X/1). JJM acknowledges an International Engagement Travel Grant from Durham University. The data presented in this paper are available from <http://dx.doi.org/10.15128/r16d56zw600>.

-
- [1] M. Baranov, L. Dobrek, K. G3ral, L. Santos, and M. Lewenstein, *Phys. Scr.* **2002**, 74 (2002).
 - [2] H. P. B3uchler, E. Demler, M. Lukin, A. Micheli, N. Prokof'ev, G. Pupillo, and P. Zoller, *Phys. Rev. Lett.* **98**, 060404 (2007).
 - [3] N. R. Cooper and G. V. Shlyapnikov, *Phys. Rev. Lett.* **103**, 155302 (2009).
 - [4] R. V. Krems, *Phys. Chem. Chem. Phys.* **10**, 4079 (2008).
 - [5] S. Ospelkaus, K.-K. Ni, D. Wang, M. De Miranda, B. Neyenhuis, G. Qu3m3ener, P. Julienne, J. Bohn, D. Jin, and J. Ye, *Science* **327**, 853 (2010).
 - [6] V. V. Flambaum and M. G. Kozlov, *Phys. Rev. Lett.* **99**, 150801 (2007).
 - [7] E. R. Meyer and J. L. Bohn, *Phys. Rev. A* **80**, (2009).
 - [8] T. A. Isaev, S. Hoekstra, and R. Berger, *Phys. Rev. A* **82**, 052521 (2010).
 - [9] J. Hudson, D. Kara, I. Smallman, B. Sauer, M. Tarbutt, and E. Hinds, *Nature* **473**, 493 (2011).
 - [10] M. S. Safronova, D. Budker, D. DeMille, D. F. J. Kimball, A. Derevianko, and C. W. Clark, *arXiv:1710.01833*.
 - [11] R. Barnett, D. Petrov, M. Lukin, and E. Demler, *Phys. Rev. Lett.* **96**, 190401 (2006).
 - [12] A. V. Gorshkov, S. R. Manmana, G. Chen, J. Ye, E. Demler, M. D. Lukin, and A. M. Rey, *Phys. Rev. Lett.* **107**, 115301 (2011).
 - [13] J. L. Bohn, A. M. Rey, and J. Ye, *Science* **357**, 1002 (2017).
 - [14] D. DeMille, *Phys. Rev. Lett.* **88**, 067901 (2002).
 - [15] L. D. Carr, D. DeMille, R. V. Krems, and J. Ye, *New J. Phys.* **11**, 055049 (2009).
 - [16] M. A. Baranov, M. Dalmonte, G. Pupillo, and P. Zoller, *Chem. Rev.* **112**, 5012 (2012).
 - [17] M. T. Hummon, M. Yeo, B. K. Stuhl, A. L. Collopy, Y. Xia, and J. Ye, *Phys. Rev. Lett.* **110**, 143001 (2013).
 - [18] M. H. Steinecker, D. J. McCarron, Y. Zhu, and D. DeMille, *ChemPhysChem* **17**, 3664 (2016).

- [19] I. Kozyryev, L. Baum, K. Matsuda, B. L. Augenbraun, L. Anderegg, A. P. Sedlack, and J. M. Doyle, *Phys. Rev. Lett.* **118**, 173201 (2017).
- [20] S. Truppe, H. J. Williams, M. Hambach, L. Caldwell, N. J. Fitch, E. A. Hinds, B. E. Sauer, and M. R. Tarbutt, *Nat. Phys.* **13**, 1173 (2017).
- [21] K.-K. Ni, S. Ospelkaus, M. De Miranda, A. Pe'er, B. Neyenhuis, J. Zirbel, S. Kotochigova, P. Julienne, D. Jin, and J. Ye, *Science* **322**, 231 (2008).
- [22] T. Takekoshi, L. Reichsöllner, A. Schindewolf, J. M. Hutson, C. R. Le Sueur, O. Dulieu, F. Ferlaino, R. Grimm, and H.-C. Nägerl, *Phys. Rev. Lett.* **113**, 205301 (2014).
- [23] P. K. Molony, P. D. Gregory, Z. Ji, B. Lu, M. P. Köppinger, C. R. Le Sueur, C. L. Blackley, J. M. Hutson, and S. L. Cornish, *Phys. Rev. Lett.* **113**, 255301 (2014).
- [24] J. W. Park, S. A. Will, and M. W. Zwierlein, *Phys. Rev. Lett.* **114**, 205302 (2015).
- [25] M. Guo, B. Zhu, B. Lu, X. Ye, F. Wang, R. Vexiau, N. Bouloufa-Maafa, G. Quémener, O. Dulieu, and D. Wang, *Phys. Rev. Lett.* **116**, 205303 (2016).
- [26] B. Yan, S. A. Moses, B. Gadway, J. P. Covey, K. R. A. Hazzard, A. M. Rey, D. S. Jin, and J. Ye, *Nature* **501**, 521 (2013).
- [27] J. W. Park, Z. Z. Yan, H. Loh, S. A. Will, and M. W. Zwierlein, *Science* **357**, 372 (2017).
- [28] J. A. Blackmore, L. Caldwell, P. D. Gregory, E. M. Bridge, R. Sawant, J. Aldegunde, J. Mur-Petit, D. Jaksch, J. M. Hutson, B. E. Sauer, M. R. Tarbutt, and S. L. Cornish, *arXiv:1804.02372*.
- [29] S. Tassy, N. Nemitz, F. Baumer, C. Höhl, A. Batär, and A. Görlitz, *J. Phys. B: At., Mol. Opt. Phys.* **43**, 205309 (2010).
- [30] H. Hara, Y. Takasu, Y. Yamaoka, J. M. Doyle, and Y. Takahashi, *Phys. Rev. Lett.* **106**, 205304 (2011).
- [31] B. Pasquiou, A. Bayerle, S. M. Tzanova, S. Stellmer, J. Szczepkowski, M. Parigger, R. Grimm, and F. Schreck, *Phys. Rev. A* **88**, 023601 (2013).
- [32] R. Roy, A. Green, R. Bowler, and S. Gupta, *Phys. Rev. Lett.* **118**, 055301 (2017).
- [33] A. S. Flores, H. P. Mishra, W. Vassen, and S. Knoop, *Eur. Phys. J. D* **71**, 49 (2017).
- [34] M. Witkowski, B. Nagórny, R. Munoz-Rodriguez, R. Ciuryło, P. S. Żuchowski, S. Bilicki, M. Piotrowski, P. Morzyński, and M. Zawada, *Opt. Express* **25**, 3165 (2017).
- [35] T. M. Rvachov, H. Son, A. T. Sommer, S. Ebadi, J. J. Park, M. W. Zwierlein, W. Ketterle, and A. O. Jamison, *Phys. Rev. Lett.* **119**, 143001 (2017).
- [36] A. Micheli, G. Pupillo, H. P. Büchler, and P. Zoller, *Phys. Rev. A* **76**, 043604 (2007).
- [37] E. Abrahamsson, T. V. Tscherbul, and R. V. Krems, *J. Chem. Phys.* **127**, 044302 (2007).
- [38] P. S. Żuchowski, J. Aldegunde, and J. M. Hutson, *Phys. Rev. Lett.* **105**, 153201 (2010).
- [39] D. A. Brue and J. M. Hutson, *Phys. Rev. Lett.* **108**, 043201 (2012).
- [40] D. A. Brue and J. M. Hutson, *Phys. Rev. A* **87**, 052709 (2013).
- [41] V. Barbé, A. Ciamei, B. Pasquiou, L. Reichsöllner, F. Schreck, P. S. Żuchowski, and J. M. Hutson, *arXiv:1710.03093*.
- [42] K. M. Jones, E. Tiesinga, P. D. Lett, and P. S. Julienne, *Rev. Mod. Phys.* **78**, 483 (2006).
- [43] K. Bergmann, H. Theuer, and B. W. Shore, *Rev. Mod. Phys.* **70**, 1003 (1998).
- [44] A. J. Kerman, J. M. Sage, S. Sainis, T. Bergeman, and D. DeMille, *Phys. Rev. Lett.* **92**, (2004).
- [45] J. M. Sage, S. Sainis, T. Bergeman, and D. DeMille, *Phys. Rev. Lett.* **94**, (2005).
- [46] J. Deiglmayr, A. Grochola, M. Repp, K. Mörtlbauer, C. Glück, J. Lange, O. Dulieu, R. Wester, and M. Weidemüller, *Phys. Rev. Lett.* **101**, 133004 (2008).
- [47] P. Zabawa, A. Wakim, M. Haruza, and N. P. Bigelow, *Phys. Rev. A* **84**, 061401 (2011).
- [48] A. Altaf, S. Dutta, J. Lorenz, J. Pérez-Ríos, Y. P. Chen, and D. S. Elliott, *J. Chem. Phys.* **142**, 114310 (2015).
- [49] S. Stellmer, B. Pasquiou, R. Grimm, and F. Schreck, *Phys. Rev. Lett.* **109**, 115302 (2012).
- [50] A. Ciamei, A. Bayerle, C.-C. Chen, B. Pasquiou, and F. Schreck, *Phys. Rev. A* **96**, 013406 (2017).
- [51] K. Aikawa, D. Akamatsu, M. Hayashi, K. Oasa, J. Kobayashi, P. Naidon, T. Kishimoto, M. Ueda, and S. Inouye, *Phys. Rev. Lett.* **105**, 203001 (2010).
- [52] D. N. Meniaïlava and M. B. Shundalau, *Comput. Theor. Chem.* **1111**, 20 (2017).
- [53] S. L. Kemp, K. L. Butler, R. Freytag, S. A. Hopkins, E. A. Hinds, M. R. Tarbutt, and S. L. Cornish, *Rev. Sci. Instrum.* **87**, 023105 (2016).
- [54] S. A. Hopkins, K. Butler, A. Guttridge, S. Kemp, R. Freytag, E. A. Hinds, M. R. Tarbutt, and S. L. Cornish, *Rev. Sci. Instrum.* **87**, 043109 (2016).
- [55] A. Guttridge, S. Hopkins, S. Kemp, D. Boddy, R. Freytag, M. Jones, M. Tarbutt, E. Hinds, and S. Cornish, *J. Phys. B: At., Mol. Opt. Phys.* **49**, 145006 (2016).
- [56] A. Guttridge, S. A. Hopkins, S. L. Kemp, M. D. Frye, J. M. Hutson, and S. L. Cornish, *Phys. Rev. A* **96**, 012704 (2017).
- [57] In addition to dipole matrix elements, the strengths of molecular transitions are subject to further effects such as the Franck-Condon overlap and rotational couplings.
- [58] R. W. P. Drever, J. L. Hall, F. V. Kowalski, J. Hough, G. M. Ford, A. J. Munley, and H. Ward, *Appl. Phys. B* **31**, 97 (1983).
- [59] J. I. Thorpe, K. Numata, and J. Livas, *Opt. Express* **16**, 15980 (2008).
- [60] P. D. Gregory, P. K. Molony, M. P. Köppinger, A. Kumar, Z. Ji, B. Lu, A. L. Marchant, and S. L. Cornish, *New J. Phys.* **17**, 055006 (2015).
- [61] M. Berninger, A. Zenesini, B. Huang, W. Harm, H.-C. Nägerl, F. Ferlaino, R. Grimm, P. S. Julienne, and J. M. Hutson, *Phys. Rev. A* **87**, (2013).
- [62] M. Pichler, H. Chen, and W. C. Stwalley, *J. Chem. Phys.* **121**, 1796 (2004).
- [63] L. Pruvost and H. Jelassi, *J. Phys. B: At., Mol. Opt. Phys.* **43**, 125301 (2010).
- [64] J. Ma, W. Liu, J. Yang, J. Wu, W. Sun, V. S. Ivanov, A. S. Skublov, V. B. Sovkov, X. Dai, and S. Jia, *J. Chem. Phys.* **141**, 244310 (2014).
- [65] W. Liu, R. Xu, J. Wu, J. Yang, S. S. Lukashov, V. B. Sovkov, X. Dai, J. Ma, L. Xiao, and S. Jia, *J. Chem. Phys.* **143**, 124307 (2015).
- [66] P. Li, W. Liu, J. Wu, J. Ma, Q. Fan, L. Xiao, W. Sun, and S. Jia, *J. Quant. Spectrosc. Radiat. Transfer* **196**, 176 (2017).
- [67] B. L. Tolra, N. Hoang, B. T'Jampens, N. Vanhaecke, C. Drag, A. Crubellier, D. Comparat, and P. Pillet, *Europhys. Lett.* **64**, 171 (2003).

- [68] P. Pellegrini, M. Gacesa, and R. Côté, *Phys. Rev. Lett.* **101**, (2008).
- [69] M. Junker, D. Dries, C. Welford, J. Hitchcock, Y. P. Chen, and R. G. Hulet, *Phys. Rev. Lett.* **101**, (2008).
- [70] R. S. Mulliken, *Rev. Mod. Phys.* **2**, 60 (1930).
- [71] A. Carrington, C. H. Pyne, A. M. Shaw, S. M. Taylor, J. M. Hutson, and M. M. Law, *J. Chem. Phys.* **105**, 8602 (1996).
- [72] N. Nemitz, F. Baumer, F. Münchow, S. Tassy, and A. Görlitz, *Phys. Rev. A* **79**, 061403 (2009).
- [73] C. Bruni and A. Görlitz, *Phys. Rev. A* **94**, (2016).
- [74] I. G. Hughes and T. P. A. Hase, *Measurements and their Uncertainties* (Oxford University Press, 2010).
- [75] T. Udem, J. Reichert, R. Holzwarth, and T. W. Hänsch, *Phys. Rev. Lett.* **82**, 3568 (1999).
- [76] R. J. LeRoy and R. B. Bernstein, *J. Chem. Phys.* **52**, 3869 (1970).
- [77] D. Comparat, *J. Chem. Phys.* **120**, 1318 (2004).
- [78] M. Borkowski, P. Morzyński, R. Ciuryło, P. S. Julienne, M. Yan, B. J. DeSalvo, and T. C. Killian, *Phys. Rev. A* **90**, 032713 (2014).
- [79] D. A. Steck, “Cesium D line data, available online at <http://steck.us/alkalidata> (revision 2.1.4),” (2010).
- [80] Y. Takasu, K. Maki, K. Komori, T. Takano, K. Honda, M. Kumakura, T. Yabuzaki, and Y. Takahashi, *Phys. Rev. Lett.* **91**, 040404 (2003).
- [81] T. Fukuhara, S. Sugawa, and Y. Takahashi, *Phys. Rev. A* **76**, 051604 (2007).
- [82] T. Fukuhara, Y. Takasu, M. Kumakura, and Y. Takahashi, *Phys. Rev. Lett.* **98**, 030401 (2007).
- [83] Y. Takasu and Y. Takahashi, *J. Phys. Soc. Jpn.* **78**, 012001 (2009).
- [84] S. Taie, Y. Takasu, S. Sugawa, R. Yamazaki, T. Tsujimoto, R. Murakami, and Y. Takahashi, *Phys. Rev. Lett.* **105**, 190401 (2010).
- [85] S. Sugawa, R. Yamazaki, S. Taie, and Y. Takahashi, *Phys. Rev. A* **84**, 011610 (2011).
- [86] M. Kitagawa, K. Enomoto, K. Kasa, Y. Takahashi, R. Ciuryło, P. Naidon, and P. S. Julienne, *Phys. Rev. A* **77**, 012719 (2008).